



UNIVERSITY OF LEEDS

This is a repository copy of *Generating ultrafast pulses of light from quantum cascade lasers*.

White Rose Research Online URL for this paper:
<http://eprints.whiterose.ac.uk/91489/>

Version: Accepted Version

Article:

Wang, F, Maussang, K, Moumdji, S et al. (9 more authors) (2015) Generating ultrafast pulses of light from quantum cascade lasers. *Optica*, 2 (11). pp. 944-949. ISSN 2334-2536

<https://doi.org/10.1364/OPTICA.2.000944>

Reuse

Items deposited in White Rose Research Online are protected by copyright, with all rights reserved unless indicated otherwise. They may be downloaded and/or printed for private study, or other acts as permitted by national copyright laws. The publisher or other rights holders may allow further reproduction and re-use of the full text version. This is indicated by the licence information on the White Rose Research Online record for the item.

Takedown

If you consider content in White Rose Research Online to be in breach of UK law, please notify us by emailing eprints@whiterose.ac.uk including the URL of the record and the reason for the withdrawal request.



eprints@whiterose.ac.uk
<https://eprints.whiterose.ac.uk/>

Generating ultrafast pulses of light from quantum cascade lasers

Feihu Wang¹, Kenneth Maussang¹, Souad Moudjji², Raffaele Colombelli², Joshua R. Freeman³, Iman Kundu³, Lianhe Li³, Edmund H. Linfield³, A. Giles Davies³, Juliette Mangeney¹, Jérôme Tignon¹ & Sukhdeep S. Dhillon^{1,*}

¹ *Laboratoire Pierre Aigrain, Ecole Normale Supérieure-PSL Research University, CNRS, Université Pierre et Marie Curie-Sorbonne Universités, Université Paris Diderot-Sorbonne Paris Cité, 24 rue Lhomond, 75231 Paris Cedex 05, France*

² *Institut d'Electronique Fondamentale, UMR 8622 CNRS, Université Paris-Saclay, 91405 Orsay, France*

³ *School of Electronic and Electrical Engineering, University of Leeds, Woodhouse Lane, Leeds LS29JT, UK*

The generation of ultrashort pulses from quantum cascade lasers (QCLs) has proved to be challenging. It has been suggested that the ultrafast electron dynamics of these devices is the limiting factor for modelocking and hence pulse formation. Even so, clear modelocking of terahertz (THz) QCLs has been recently demonstrated but the exact mechanism for pulse generation is not fully understood. Here we demonstrate that the dominant factor necessary for active pulse generation is in fact the synchronization between the propagating electronic modulation and the generated THz pulse in the QCL. By using phase resolved detection of the electric field in QCLs embedded in metal-metal waveguides, we demonstrate that active modelocking requires the phase velocity of the microwave round trip modulation to equal the group velocity of the THz pulse. This allows the THz pulse to propagate in phase with the microwave modulation along the gain medium, permitting short pulse generation. Modelocking was performed on QCLs employing phonon depopulation active regions, permitting coherent detection of large gain bandwidths (500 GHz), and the generation of 11 ps pulses centered around 2.6 THz when the above ‘phase-matching’ condition is satisfied. This work brings an enhanced understanding of QCL modelocking and will permit new concepts to be explored to generate shorter and more intense pulses from mid-infrared, as well as THz, QCLs.

1. INTRODUCTION

Terahertz (THz) frequency quantum cascade lasers (QCLs) [1] are semiconductor devices based on intersubband transitions that can emit over the $\sim 1 - 5$ THz spectral range. There has been considerable developments in the performance of these sources over recent years, including significant increases in output power [2] and operating temperature [3]. Since the ultrafast gain recovery time inherent to QCLs is considerably shorter than the round-trip cavity time [4], it has been believed that these devices cannot be modelocked (multiple pulses are generated within the QCL cavity) and thus unable to generate short pulses. However, it has recently been shown that these devices can be actively modelocked, where the QCL is modulated at microwave frequencies, to generate a train of picosecond pulses [4] [5] [6]. Nonetheless, the exact mechanism that permits pulse generation is not fully understood, unlike interband lasers where active modelocking has been extensively investigated and is well known [7] [8] [9]. For example, it is not clear why THz QCLs are easier to modelock when compared to those operating in the mid-infrared. A further challenge to understanding QCL modelocking in the THz frequency range is that all demonstrations to date have been based on QCLs employing bound-to-continuum active region designs and fabricated in single plasmon waveguides. These active regions were used as they have low electrical power requirements thus permitting continuous wave (CW) operation (or high duty cycles) whilst the single plasmon waveguides help provide high output powers. However, this has restricted insight into the modelocking mechanism. For example, this active region leads to small spectral bandwidths (~ 100 GHz), and so the effect of the bandwidth on the pulse generation has not been investigated. Furthermore, no consideration has been made on the suitability of the single plasmon THz waveguide for guiding the microwave modulation.

In this article, we demonstrate active modelocking through injection seeding of THz QCLs based on the longitudinal-optical (LO) phonon depopulation active region scheme, embedded in metal-metal (MM) waveguides. These active regions provide large emission bandwidths, greater than 500 GHz, and the MM waveguide confines both the microwave modulation and THz emission. Using this large bandwidth, we demonstrate that the actively modelocked pulse width is principally determined by the microwave frequency modulation, rather than being limited by the gain bandwidth, and show that the microwave phase velocity needs to be equal to the THz group velocity for pulse generation. The active modelocking method reported here, in contrast to modelocking demonstrations of reference [5], also limits pulse generation close to the lasing threshold owing to the direct modulation of the gain above and below threshold through the entire cavity. The fast direct modulation is permitted by the ultrafast gain recovery time which we determine experimentally to be ~ 5 ps, approaching that of mid-infrared QCLs (~ 1 ps).

2. SAMPLE

A QCL with a LO phonon depopulation scheme was used, based on a 3.1 THz QCL that has been shown to operate up to 200 K [3]. The design was modified to operate at lower frequencies (~ 2.6 THz) by increasing the well and barrier widths, thereby improving the spectral overlap with the THz seed pulse [10]. Starting from the injection barrier, the well and barrier widths were *4.6/9.8/2.6/9.0/4.4/17.6* nm (barriers in italic). The 17.6-nm-wide well was n-doped at a level of 5×10^{16} cm⁻³ over the central 5 nm.

The growth was performed using molecular beam epitaxy. The wafer was processed into 3-mm-long laser ridges in MM waveguides using standard photolithography. This type of waveguide, coupled with the LO phonon depopulation active region design, provides state-of-the-art

THz QCL temperature performance. Ridge widths of 60 μm were selected to suppress higher lateral modes such that the fundamental mode dominates the laser action [11] important for active modelocking to avoid multiple pulses within the cavity. The QCL was coupled with a high-speed mount for GHz frequency modulation (see inset to Fig. 4c) and placed in a continuous flow cryostat. At 77K, the laser threshold is observed at 722 A/cm² and lasing ceases at 998 A/cm² with a duty cycle of 6 %. Fig. 1 shows the light-current-voltage (LIV) characteristics of the QCL, using a pyroelectric detector to measure the output power. Laser action is observed up to 130 K with a duty cycle of 6 %. The electrical characteristics are typical for this type of active region. The inset to Fig. 1 shows the calculated mode profiles in facet and surface views confirming that only one lateral mode is present.

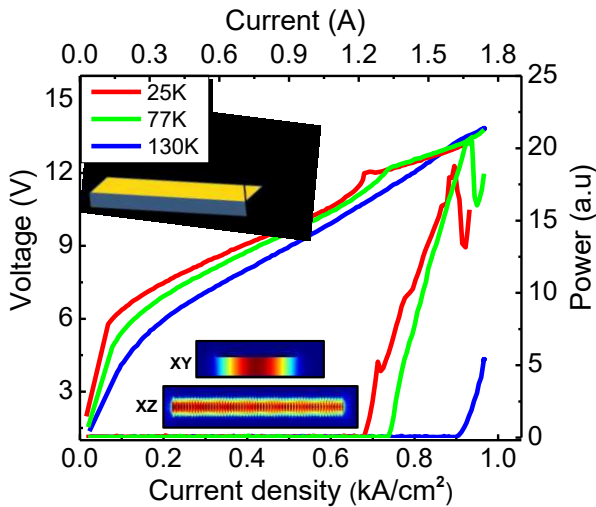


Fig. 1. Light-current density-voltage characteristics of the 2.6 THz metal-metal waveguide QCL based on a longitudinal optical phonon depopulation active region at 25 K (red), 77 K (green) and 130 K (blue). Top inset: schematic diagram showing the QCL coordinate system XYZ. Bottom inset: transverse (XY) and longitudinal mode (XZ) simulations of the THz mode-profile inside the metal-metal waveguided QCL.

3. INJECTION SEEDING

Prior to modelocking, a technique based on ultrafast injection seeding was employed to measure the time resolved electric field emitted by the QCL. THz frequency pulses, of bandwidth ~ 3 THz, were generated using a photoconductive antenna excited by 100 fs near-infrared pulses (centred at ~ 800 nm) from a Ti:Sapphire laser. These free-space THz pulses were injected into the MM QCL cavities using high numerical aperture parabolic mirrors, enabling injection seeding of the QCL, and permitting coherent detection of its emission. The THz pulse injection is synchronised with an electrical RF pulse that switches on the QCL, triggered by the same 100 fs near-infrared pulses. This allows the THz input pulses to be amplified and eventually seed the QCL emission, rather than the emission being initiated by the QCL's inherent spontaneous emission. Electro-optic sampling was then used to measure the amplitude and phase of the QCL emission. Further details of the technique can be found in ref [10]. (The time resolved output intensity of an unseeded QCL can be measured using a cross-polarizer technique [12] but is orders of magnitude

less sensitive compared to the seeded technique. It is thus not suited to the low output power of metal-metal QCLs).

Fig. 2(a) shows the measured electric field as a function of time for a QCL injected with an ultrafast THz seed pulse, at 77 K. The QCL was held below threshold with a quasi-DC current of 609 A/cm² with a 3.6 ns electrical switching pulse used to bring the QCL above threshold, the latter synchronised with the THz seed pulse. The seeding THz pulse is injected into the QCL through one of its facets at $t = 64$ ps and is amplified as it propagates along the laser cavity. At the output facet, part of the pulse is transmitted and coherently detected, while the remainder is reflected back into the cavity and continues to be amplified. The pulse is again reflected at the input facet. This results in successive pulses exiting the QCL output facet that increase in field amplitude, separated by the cavity round trip time of 76ps corresponding to a refractive index of 3.665. Subsequently (> 300 ps), a complex behaviour emerges with weaker emission observed between the round trip pulses, as previously seen in bound-to-continuum devices [10] [13]. This is a result of a number of longitudinal modes present in a long cavity [14] and the ultrafast gain recovery time (see below). Furthermore, owing to the finite gain bandwidth of the QCL, the input THz pulse is broadened in time with the number of roundtrips resulting in the output pulses becoming less distinguishable at later times (> 400 ps). A magnified view of the output emission around 430 ps is highlighted in Fig. 2(b) that clearly shows the time resolved form of the electric field with a resolution of 30 fs. (The inter-round trip pulses can be inhibited when using active modelocking as detailed below).

After ~ 400 ps, corresponding to six round trips, there is no further amplification of the output electric field. (The small reduction in amplitude after 700 ps is a result of the electrical switching pulse not being perfectly flat). Although the stabilization of the field is an indication that the QCL is entirely synchronised with the input pulse, the variation of the output field was investigated as a function of input THz field to confirm this. Fig. 2(c) shows the QCL output field at a time of 431 ps as a function of voltage on the THz antenna, with similar behavior observed for later times. (The electric field emitted by the antenna is proportional to applied voltage [10]). For applied fields greater than ~ 2 V, the QCL output field saturates implying that the QCL gain is clamped by the THz input pulses, with the latter therefore initiating (i.e. seeding) the laser action, replacing entirely the inherently random spontaneous emission of the QCL. (A small unsynchronized part of the electric field may still be present but this will be considerably smaller than the synchronized field [13] and, in the case of modelocking, will have a similar time profile [12]). For antenna voltages < 2 V, however, the measured QCL output field depends on the input THz pulse amplitude. This implies that only amplification of the input THz pulse is detected with contributions to the QCL output from the seed and spontaneous emission [13].

Fig. 2(d) shows the fast Fourier transform (FFT) of the measured time-domain signal in Fig. 2(a), permitting access to the QCL output spectrum. The spectrum is centered at ~ 2.6 THz with a bandwidth greater than 500 GHz, considerably larger than in previous demonstrations (100GHz) owing to the large spectral gain of LO phonon depopulation active region designs. The mode spacing is 13.2 GHz as expected for a 3-mm-long waveguide. Furthermore, the frequency of each Fabry-Perot mode is linear with mode number demonstrating that the QCL is operating on only one lateral mode and there are no higher

order modes present. The microwave beat note was also measured which showed a narrow linewidth at only one frequency at the round trip just above laser threshold, which gradually became wider with increasing current. Similar behavior of the beatnote has been previously demonstrated in, for example, reference [15].

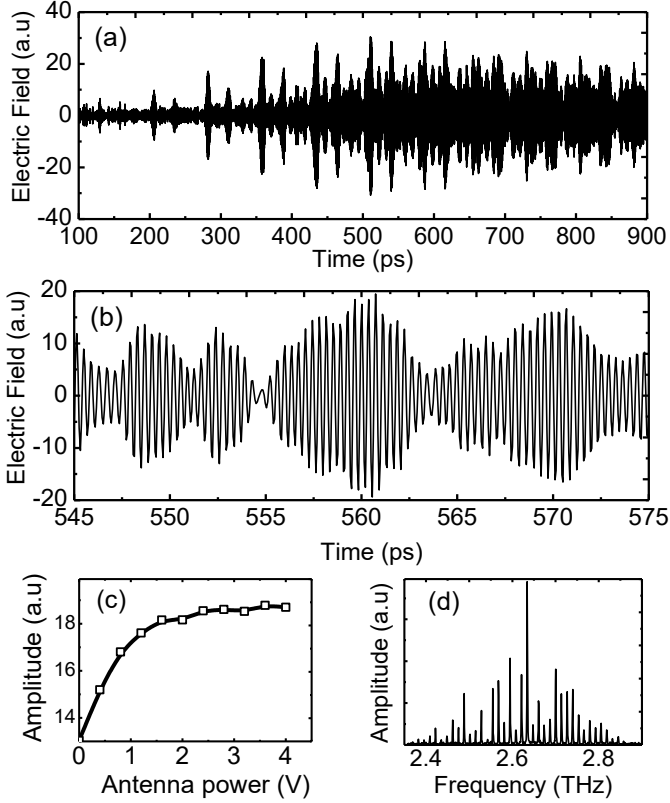


Fig. 2. Injection seeding of the metal-metal waveguide QCL at 77 K. (a) Emitted electric field from the QCL as a function of time with an bias of 3V on the seed antenna. b) Expanded view of the emitted QCL electric field between 545 ps and 575 ps. (c) QCL output field amplitude at 431 ps as a function of voltage applied of the THz photoconductive antenna. (d) FFT of the QCL output electric field.

By comparing the measured time profile in Fig. 2(a) to Maxwell-Bloch time-domain simulations, an estimate of the gain recovery time of the QCL can be obtained. Using the procedure presented in ref [14] with a dephasing time of 0.6 ps and total waveguide loss of 12 cm^{-1} , a gain recovery time of $\sim 5 \text{ ps}$ is determined. Further details of the parameters used can be found in the supplementary material 1. This is considerably faster than for bound-to-continuum devices, which have gain recovery times of $\sim 15 \text{ ps}$, and is considerably shorter than the round trip time (76 ps). (Note that the gain recovery time for mid-infrared QCLs is on the order of $\sim 1 \text{ ps}$ [16] [17]). The shorter gain recovery time is also indicated in the time resolved electric field (Fig. 2b) that shows multiple ‘pulses’ between cavity round trips separated between 5 to 7 ps. This is a result of the faster dynamics of the LO phonon depopulation designs and owing to the absence of a miniband for inter-period transport.

4. ACTIVE MODELOCKING

Using this injection seeding technique, modelocking of QCLs was investigated with the expectation that the large bandwidth available in these devices should lead to shorter pulses in comparison with modelocked bound-to-continuum active region designs [6]. Specifically, pulses as short as 1 ps would be expected from a seeding bandwidth of 500GHz, assuming transform limited pulses. To actively modelock the QCL, a microwave modulation was applied corresponding to the round trip time (i.e. $\sim 13 \text{ GHz}$ for a 3 mm long cavity) to modulate the gain across the entire gain medium. (Note that it is also possible to modulate a short section of the cavity at the round-trip frequency to actively modelock a QCL to open a picosecond time window in the net gain, as in reference [4]). However, this requires a specially designed QCL with a long gain recovery time). The position of the bonding wire on top of the QCL is placed close to the facet onto which the external THz pulse is incident (see inset to Fig. 4(c)). In this case the microwave modulation will propagate between the input and the output facets together with the seed pulse, allowing the QCL to be seeded and modelocked for pulse generation. No pulse generation is observed when the bonding wire is placed in the middle of QCL cavity as this results in a counter-propagating modulation.

The experimental arrangement for active modelocking is the same as that reported in ref [6], where a yttrium iron garnet (YIG) bandpass filter is employed to choose a harmonic of the reference laser repetition rate (for example, the 163 harmonic $\times 76.47 \text{ MHz} = 12.46 \text{ GHz}$) to synchronize the roundtrip microwave modulation of the QCL with the seeding pulses. A microwave power of 30dBm was used. This is the maximum available in our current set-up and showed the clearest pulse behavior (see below). The modulation frequency was varied between 12.4 GHz and 14 GHz with 12.465 GHz giving the best quality pulses. Fig. 3 shows the output electric fields and corresponding spectra for various modulation frequencies (RF power $\sim 500 \text{ mW}$) that show that the pulse behavior becomes clearer and more Fabry Perot modes appear as the microwave frequency is reduced. No clear pulse behavior was observed for frequencies greater than 12.7 GHz.

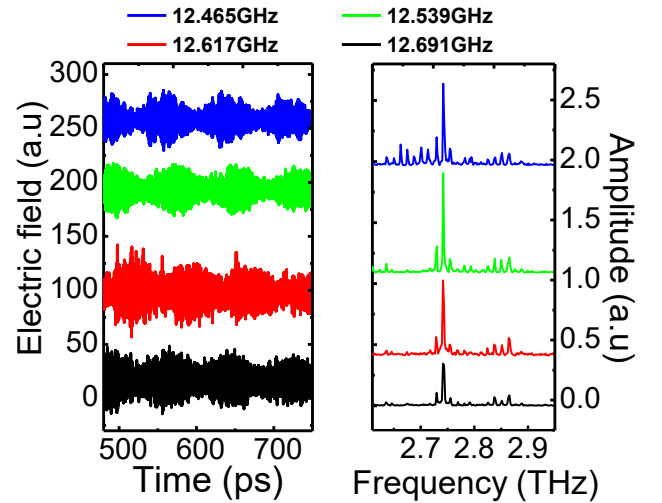


Fig. 3. QCL output electric field and corresponding spectrum for microwave modulation frequencies of 12.465 GHz, 12.539 GHz, 12.617 GHz and 12.691 GHz.

Fig. 4(a) shows the electric field between 1100 ps and 1800 ps emitted by the seeded QCL with (black curve) and without (red curve) microwave modulation. The QCL was operated at 77 K and the electrical pulse power chosen such that it brought the QCL above laser threshold. (Compared to Fig. 3, the electrical pulse power was reduced to 450 mW which lead to shorter pulses and with the pulse behavior was lost for other modulation frequencies). As in Fig. 2, the output of the QCL without microwave modulation shows a quasi-continuous profile, resulting in only two modes visible in the FFT (Fig. 4(b)). (The QCL is close to threshold limiting the number of modes generated). The situation changes drastically upon applying the microwave modulation with the clear generation of a pulse train. (The variation in intensity between pulses in the time domain is a result of the non-flat RF electrical pulses and the low output fields of MM QCLs resulting in a low signal, close to the noise level). The FFT shows the corresponding effect on the spectrum; eight uniformly spaced modes are observed between 2.61 THz and 2.72 THz. The average pulse width (in intensity) is found to be 11 ps as shown in the inset of Fig. 4(a). The number of modes and the pulse widths are larger and shorter, respectively, than those demonstrated from our previous investigations on bound-to-continuum active regions, showing the effect of the broader gain bandwidth of LO depopulation active region designs. However, the entire ~ 500 GHz bandwidth is not fully used. This is a result of the microwave modulation, which limits the pulse width and the number of modes – pulse formation is only present close to laser threshold owing to the direct sinusoidal modulation of the QCL gain above and below laser threshold (i.e. turning on and off the QCL rapidly), which limits the number of modes that can be brought above threshold. Applying this microwave modulation when the quasi DC current or the RF power supplying the QCL is closer to or above laser threshold results in a sinusoidal amplitude modulation of the detected field, owing to the finite microwave power, with the pulse behavior destroyed [12].

The application of a round trip modulation of 12.47 GHz for the shortest pulse generation is different from the mode spacing found in the QCL seeding and the beat note frequency ($\Delta\nu \sim 13.2$ GHz). From the mode spacing, we find THz group refractive indices of 3.871 and 3.665 for the modelocked and seeded regime, respectively. It has been previously shown that the QCL round-trip can be locked to an RF synthesiser over a locking range of several hundred MHz with moderate microwave powers (“injection pulling”) but it is a surprise that the 12.47 GHz modulation frequency generates the clearest pulses. This effect has also been observed in the THz spectra of microwave modulated QCLs of reference [18] where more modes are brought above threshold when a microwave modulation different from the round-trip frequency is applied. In our previous work on single plasmon waveguides, pulses were generated over a wide range of round-trip modulations (12.5 – 13.3 GHz). The difference here comes from the metal-metal waveguide which brings an extra dispersion in the refractive index of the microwave modulation and permits a THz-GHz phase matching [19], where the effective microwave index is equal to the THz group refractive index i.e. $n_c(\text{THz}) = n_{\text{eff}}(\text{GHz})$. Although this phase matching has been discussed in the context of modulation bandwidth, its demonstration and impact on short pulse generation had not been envisaged. The microwave index depends strongly on the ridge width and microwave frequency [19], with a refractive index of approximately 3.9 for a 60- μm -wide ridge at 12 GHz (see

supplementary material 2 for a simulation of microwave mode and refractive index dispersion). This indicates that the velocity of the THz pulse envelope is dictated by the microwave modulation wave and it is this direct modulation close to threshold that permits pulse generation. This phenomena is also supported by the fact that pulse generation is only observed when the microwave modulation is applied from the cavity end of the QCL, suggesting that the microwave propagates in-phase with the THz pulse. This also explains why it is easier to modelock THz QCLs in comparison with mid-infrared QCLs as, for the latter, the group refractive index is smaller (~ 3.3) than in the THz range and thus a microwave modulation has a different velocity to the mid-infrared group velocity.

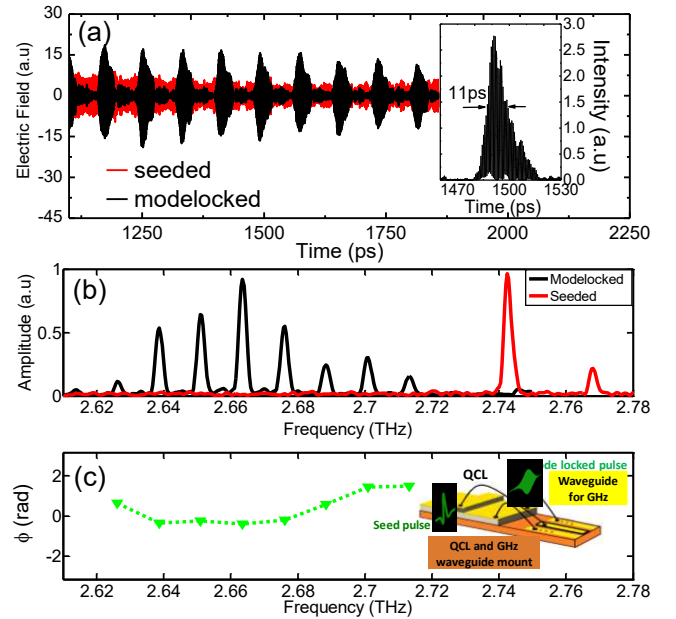


Fig. 4. Active modelocking and phase analysis of the metal-metal QCL at 77 K. (a) Output electric field for the seeded (red) and the modelocked (black) QCL with an applied 12.46 GHz microwave modulation for the latter. Inset: expanded view of the THz pulse intensity between 1470 ps and 1530 ps. (b) FFT of Fig. (a) for a seeded (red) and modelocked (black) QCL. (c) Phases of the eight modelocked longitudinal modes (green triangles). Inset: QCL schematic showing the device integrated with a microwave waveguide for active modelocking and illustrating the input seed pulse and the seeded/modelocked output.

An advantage of injection seeding with phase resolved pulses is that it permits access to the phase and amplitude of the emitted pulse train, allowing a complete analysis of the modelocked pulse emission. As can be seen in Fig. 4(a), the modelocked pulses are deformed from an ideal Gaussian profile. Taking the FFT of the pulse train permits the phase of each mode to be determined as shown in Fig. 4(c); the four central intense modes at 2.639 THz, 2.651 THz, 2.664 THz, 2.676 THz have the same phase, while the phase increases monotonically for the modes (2.626 THz, 2.689 THz, 2.701 THz and 2.714 THz) that are further from the central frequency. This deforms the pulse from the transform limited case. An improved pulse shape could be obtained by engineering the gain to have a flatter profile such that the group velocity dispersion is minimized [15] and improvements to the microwave

modulation which could be distorted by the inductance from the wire bonding.

5. DISCUSSION AND CONCLUSION

Our results on the modelocking of THz QCLs in MM waveguides show that: i) clear pulse generation is only observed when the THz group index is equal to the effective modal index of the microwave modulation; ii) pulse generation is only observed close to threshold resulting in low output THz fields; and, iii) a considerable increase in the gain bandwidth does not translate into much shorter pulses. Taken together, these three points suggest that pulse generation from QCLs arises from a direct microwave modulation above and below laser threshold, and that the pulse width is limited by the sinusoidal microwave modulation. However, the ultrafast gain recovery time measured here, which we show does not limit pulse generation, can be used as an advantage to generate more intense and shorter pulses if short intense electrical pulses can be used to switch on the QCL gain. For example a Gaussian or Lorentzian profile could be used. Although difficult to generate electronically, optically generated electrical pulses using ultrafast lasers combined with ultrafast materials are feasible, and these could then be used to switch the QCL on sub-picosecond time scales. Further techniques that could circumvent the current limitations would be the application of greater microwave power for higher pulse energies and the application of hybrid modelocking techniques to shorten the pulses to sub-10 ps values [20].

To conclude, we have demonstrated seeding of THz QCLs with an LO phonon depopulation active region design, fabricated in MM waveguides. The ultrafast seeding permits access to the gain recovery time, which is shown to be faster than that in bound-to-continuum active region designs and approaches that in mid-infrared QCLs. Furthermore, we have shown that 11 ps modelocked pulses can be generated from these MM QCLs, with the pulse width determined by the microwave modulation and phase matching between the microwave phase velocity and the envelope of the THz emission. The pulse generation is not limited by the inherent QCL bandwidth. This work implies that for QCL modelocking (THz and mid-infrared), the fast gain recovery time does not limit pulse formation, as postulated in the simulations of references [17] and [20], when a strong active modulation is applied at the correct frequency. Importantly, considerations need to be made to engineer the waveguide and refractive index dispersion to achieve phase-matching. As well as pulse generation, this work could have an impact on more stable comb generation [15] [21] when referenced to a microwave modulation. Owing to the MM geometry, the output fields were low in amplitude but this could be improved considerably by the integration of planar horn antennas [22] designed for active modelocking of such structures. Further, the QCL operating temperature and electrical power dissipation are compatible with liquid nitrogen or Stirling coolers.

FUNDING SOURCES AND ACKNOWLEDGMENTS

Funding: European Union FET-Open grant ULTRAQCL 665158, ANR-12-NANO-0014 "PhaseLock", the EPSRC (UK), the EC programme (TOSCA), the Royal Society and Wolfson Foundation and the Conseil Général de l'Essonne.

See Supplement 1 and 2 for supporting content

REFERENCES

1. R. Köhler, A. Tredicucci, F. Beltram, H. E. Beere, E. H. Linfield, A. G. Davies, D. A. Ritchie, R. C. Iotti, and F. Rossi, "Terahertz semiconductor-heterostructure laser," *Nature* **417**, 156–159 (2002).
2. L. Li, L. Chen, J. Zhu, J. Freeman, P. Dean, A. Valavanis, A. G. Davies, and E. H. Linfield, "Terahertz quantum cascade lasers with > 1 W output powers," *Electron. Lett.* **50**, 309–311 (2014).
3. S. Fatholouloumi, E. Dupont, C. W. I. Chan, Z. R. Wasilewski, S. R. Laframboise, D. Ban, A. Mátyás, C. Jirauschek, Q. Hu, and H. C. Liu, "Terahertz quantum cascade lasers operating up to 200 K with optimized oscillator strength and improved injection tunneling," *Opt. Express* **20**, 3866–3876 (2012).
4. C. Y. Wang, L. Kyznetsova, V. M. Gkortsas, L. Diehl, F. X. Kartner, M. A. Belkin, A. Belyanin, X. Li, D. Ham, H. Schneider, and others, "Mode-locked pulses from mid-infrared quantum cascade lasers," *Opt. Express* **17**, 19929–12943 (2009).
5. S. Barbieri, M. Ravaro, P. Gellie, G. Santarelli, C. Manquest, C. Sirtori, S. P. Khanna, E. H. Linfield, and A. G. Davies, "Coherent sampling of active mode-locked terahertz quantum cascade lasers and frequency synthesis," *Nat. Photonics* **5**, 306–313 (2011).
6. J. R. Freeman, J. Maysonave, H. E. Beere, D. A. Ritchie, J. Tignon, and S. S. Dhillon, "Electric field sampling of modelocked pulses from a quantum cascade laser," *Opt. Express* **21**, 16162 (2013).
7. J. E. Bowers, P. Morton, A. Mar, S. W. Corzine, and others, "Actively mode-locked semiconductor lasers," *Quantum Electron. IEEE J. Of* **25**, 1426–1439 (1989).
8. E. L. Portnoi, J. H. Marsh, and E. A. Avrutin, "Monolithic and multi-GigaHertz mode-locked semiconductor lasers: Constructions, experiments, models and applications," *IEE Proc. - Optoelectron.* **147**, 251–278 (2000).
9. L. A. Jiang, M. E. Grein, H. Haus, E. P. Ippen, and others, "Noise of mode-locked semiconductor lasers," *Sel. Top. Quantum Electron. IEEE J. Of* **7**, 159–167 (2001).
10. D. Oustinov, N. Jukam, R. Rungsawang, J. Madéo, S. Barbieri, P. Filloux, C. Sirtori, X. Marcadet, J. Tignon, and S. Dhillon, "Phase seeding of a terahertz quantum cascade laser," *Nat. Commun.* **1**, 1–6 (2010).
11. W. Maineult, P. Gellie, A. Andronico, P. Filloux, G. Leo, C. Sirtori, S. Barbieri, E. Peytavit, T. Akalin, J.-F. Lampin, H. E. Beere, and D. A. Ritchie, "Metal-metal terahertz quantum cascade laser with micro-transverse-electromagnetic-horn antenna," *Appl. Phys. Lett.* **93**, - (2008).
12. J. R. Freeman, J. Maysonave, N. Jukam, P. Cavalié, K. Maussang, H. E. Beere, D. A. Ritchie, J. Mangeney, S. S. Dhillon, and J. Tignon, "Direct intensity sampling of a modelocked terahertz quantum cascade laser," *Appl. Phys. Lett.* **101**, 181115 (2012).

13. J. Maysonnave, N. Jukam, M. S. M. Ibrahim, R. Rungsawang, K. Maussang, J. Madéo, P. Cavalié, P. Dean, S. P. Khanna, D. P. Steenson, and others, "Measuring the sampling coherence of a terahertz quantum cascade laser," *Opt. Express* **20**, 16662–16670 (2012).
14. J. R. Freeman, J. Maysonnave, S. Khanna, E. H. Linfield, A. G. Davies, S. S. Dhillon, and J. Tignon, "Laser-seeding dynamics with few-cycle pulses: Maxwell-Bloch finite-difference time-domain simulations of terahertz quantum cascade lasers," *Phys. Rev. A* **87**, (2013).
15. M. Rösch, G. Scalari, M. Beck, and J. Faist, "Octave-spanning semiconductor laser," *Nat Photon* **9**, 42–47 (2015).
16. W. Kuehn, W. Parz, P. Gaal, K. Reimann, M. Woerner, T. Elsaesser, T. Müller, J. Darmo, K. Unterrainer, M. Austerer, G. Strasser, L. R. Wilson, J. W. Cockburn, A. B. Krysa, and J. S. Roberts, "Ultrafast phase-resolved pump-probe measurements on a quantum cascade laser," *Appl. Phys. Lett.* **93**, 151106 (2008).
17. Y. Wang and A. Belyanin, "Active mode-locking of mid-infrared quantum cascade lasers with short gain recovery time," *Opt. Express* **23**, 4173 (2015).
18. S. Barbieri, W. Maineult, S. S. Dhillon, C. Sirtori, J. Alton, N. Breuil, H. E. Beere, and D. A. Ritchie, "13 GHz direct modulation of terahertz quantum cascade lasers," *Appl. Phys. Lett.* **91**, 143510 (2007).
19. W. Maineult, L. Ding, P. Gellie, P. Filloux, C. Sirtori, S. Barbieri, T. Akalin, J.-F. Lampin, I. Sagnes, H. E. Beere, and D. A. Ritchie, "Microwave modulation of terahertz quantum cascade lasers: a transmission-line approach," *Appl. Phys. Lett.* **96**, 021108 (2010).
20. A. K. Wójcik, P. Malara, R. Blanchard, T. S. Mansuripur, F. Capasso, and A. Belyanin, "Generation of picosecond pulses and frequency combs in actively mode locked external ring cavity quantum cascade lasers," *Appl. Phys. Lett.* **103**, 231102 (2013).
21. A. Hugi, G. Villares, S. Blaser, H. C. Liu, and J. Faist, "Mid-infrared frequency comb based on a quantum cascade laser," *Nature* **492**, 229–233 (2012).
22. A. Brewer, J. R. Freeman, P. Cavalié, J. Maysonnave, J. Tignon, S. S. Dhillon, H. E. Beere, and D. A. Ritchie, "Coherent detection of metal-metal terahertz quantum cascade lasers with improved emission characteristics," *Appl. Phys. Lett.* **104**, 081107 (2014).